

# Connectivity Architecture and Subdivision of the Human Inferior Parietal Cortex Revealed by Diffusion MRI

Michael Ruschel<sup>1</sup>, Thomas R. Knösche<sup>1</sup>, Angela D. Friederici<sup>2</sup>, Robert Turner<sup>3</sup>, Stefan Geyer<sup>3</sup>, and Alfred Anwander<sup>1,2</sup>

<sup>1</sup>Research Group “Cortical Networks and Cognitive Functions”, <sup>2</sup>Department of Neuropsychology, <sup>3</sup>Department of Neurophysics, Max Planck Institute for Human Cognitive and Brain Sciences, Leipzig, Germany

Address correspondence to Alfred Anwander, Max Planck Institute for Human Cognitive and Brain Sciences, Stephanstrasse 1a, 04103 Leipzig, Germany. Email: anwander@cbs.mpg.de; <http://www.cbs.mpg.de/~anwander>  
Stefan Geyer and Alfred Anwander share senior authorship.

**The human inferior parietal cortex convexity (IPCC) is an important association area, which integrates auditory, visual, and somatosensory information. However, the structural organization of the IPCC is a controversial issue. For example, cytoarchitectonic parcellations reported in the literature range from 2 to 7 areas. Moreover, anatomical descriptions of the human IPCC are often based on experiments in the macaque monkey. In this study, we used diffusion-weighted magnetic resonance imaging combined with probabilistic tractography to quantify the connectivity of the human IPCC, and used this information to parcellate this cortex area. This provides a new structural map of the human IPCC, comprising 3 subareas (inferior parietal cortex anterior, IPC middle, and IPC posterior) of comparable size, in a rostro-caudal arrangement in the left and right hemispheres. Each subarea is characterized by a connectivity fingerprint, and the parcellation is similar to the subdivision reported for the macaque IPCC with 3 areas in a rostro-caudal arrangement (PF, PFG, and PG). However, the present study also reliably demonstrates new structural features in the connectivity pattern of the human IPCC, which are not known to exist in the macaque. This study quantifies intersubject variability by providing a population representation of the subarea arrangement and demonstrates the substantial lateralization of the connectivity patterns of the IPCC.**

**Keywords:** connectivity-based parcellation, diffusion MRI, diffusion tensor imaging, human parietal lobe, inferior parietal cortical convexity, probabilistic tractography

## Introduction

The human inferior parietal cortex convexity (IPCC) is an important association area, which integrates auditory, visual, and somatosensory information. This region plays a prominent role in visuo-spatial attention, especially in the right hemisphere, and in particular in the stimulus-driven ventral frontoparietal attention network. In contrast, the superior posterior parietal lobe (SPL) is (bilaterally) engaged in the more endogenously driven dorsal attention network (Corbetta and Shulman 2002). A second important area of involvement for the IPCC is in episodic memory retrieval. Paralleling the dichotomy of their involvement in the attention networks, the SPL is more associated with endogenous or voluntary processes, while the IPCC supports processes like recollection, driven by external events (Cabeza et al. 2008; Vilberg and Rugg 2008). Moreover, in the left hemisphere, the IPCC is an important constituent of the cortical language network (Sakai et al. 2001; Binder et al. 2009; Graves et al. 2010; Hartwigsen et al. 2010; Price 2010).

There is evidence that the IPCC can be further subdivided into functional subareas. For example, familiarity-based

episodic memory effects are primarily found in the rostral part of IPCC (approximately the supramarginal gyrus; Cabeza et al. 2008; Vilberg and Rugg 2008). This same rostral area is related to covert articulation and phonological decision/mapping within the language network, while the caudal part of IPCC (approximately the angular gyrus) is involved in semantic retrieval (Vigneau et al. 2006; Binder et al. 2009; Graves et al. 2010; Price 2010).

Hence, the IPCC accommodates a rich variety of cognitive functionality, which maps onto distinct functionally specialized subareas. This is likely to be paralleled by a similar structural organization of anatomically distinct subareas. However, this subdivision remains a controversial issue. Brodmann (1909), in his “classical” cytoarchitectonic map, subdivided the IPCC into 2 regions: Rostral area 40 (on the supramarginal gyrus) and caudal area 39 (on the angular gyrus). Subsequent investigators, using cytoarchitecture (von Economo and Koskinas 1925; Gerhardt 1940; Sarkisov et al. 1955) or myeloarchitecture (Vogt 1911; Batsch 1956), parcellated the IPCC into a higher number of regions, each characterized by a specific regional architectonic layout (termed “subareas” or “subregions”). A recent study (Caspers et al. 2006), using state-of-the-art observer-independent cytoarchitectonic mapping (Schleicher et al. 1999), found 7 areas in the IPCC: 5 in its rostral part (broadly equivalent to Brodmann area 40) and 2 in its caudal part (broadly equivalent to Brodmann area 39). Subsequently, Caspers et al. (2013) used receptor mapping and showed that these 7 areas could be clustered into 3 larger rostro-caudally arranged regions.

In the macaque monkey, the situation is more straightforward. The classical cyto- and myeloarchitectonic literature identified 1 (Brodmann 1909) or 2 (Vogt and Vogt 1919; von Bonin and Bailey 1947) regions. Multimodal studies employing architectonic mapping (Pandya and Seltzer 1982; Gregoriou et al. 2006), in vitro autoradiography of the distribution of neurotransmitter binding sites (Geyer et al. 2005), tract tracing (Pandya and Seltzer 1982; Rozzi et al. 2006), and electrophysiology (Rozzi et al. 2008) converge on a parcellation into 4 regions: PF, PFG, PG, and Opt—aligned in a rostro-caudal arrangement along the longitudinal axis of the IPCC. The nomenclature of the areas were proposed by Pandya and Seltzer (1982), based on the initial naming convention by von Bonin and Bailey (1947). The 4 areas markedly differ in their architectonic organization (cytoarchitecture, myeloarchitecture, regional distribution of neurotransmitter binding sites, and immunoreactivity; Geyer et al. 2005; Gregoriou et al. 2006), frontal, parietal, as well as temporal cortical connections (Rozzi et al. 2006), and in the somatosensory, visual, as well as motor responses of their neurons (Rozzi et al. 2008).

However, despite this extensive characterization, their possible homologs in humans are still unclear.

In humans, a different perspective may shed new light on this old problem: Not only cyto- or myeloarchitecture, but also connectivity patterns can structurally (and therefore, also functionally) characterize cortical areas. Diffusion-weighted magnetic resonance imaging (dMRI), combined with probabilistic tractography, elegantly measures such connectivity patterns noninvasively in living participants (Johansen-Berg et al. 2004; Anwander et al. 2007). This technique can be used to compute connectivity fingerprints that characterize the connectivity of a brain area under investigation with a collection of preselected target areas. For example, Behrens et al. (2003) parcellated the human thalamus, according to its connectivity to a number of macroanatomically defined cortical regions. More recently, Rushworth et al. (2006) used probabilistic tractography to characterize the connectivity profile of 6 predefined target regions in the lateral parietal cortex with 3 predefined regions elsewhere in the brain (superior colliculus, parahippocampal gyrus, and ventral premotor cortex), which are known to project differentially to 3 distinct regions in macaque parietal cortex. They provide a detailed comparison of the connection pathways between these areas to corresponding pathways in the macaque brain.

A different, less hypothesis driven, approach exploits the fact that probabilistic tractography is able to estimate the connectivity profile of each point in a region of interest (ROI; here the IPCC) to the rest of the brain. With an automatic clustering algorithm, cortical regions can then be identified, which feature internally coherent but mutually distinct connectivity (Anwander et al. 2007). This approach has been successfully applied to parcellate the medial premotor cortex into supplementary and presupplementary motor areas (Johansen-Berg et al. 2004), the lateral premotor cortex into its dorsal and ventral subregions (Tomassini et al. 2007; Schubotz et al. 2010), Broca's area into Brodmann areas (BA) 44 and 45 (Anwander et al. 2007; Klein et al. 2007), and the cingulate cortex into anterior, midcingulate, and posterior subregions (Beckmann et al. 2009). Very recently, Mars et al. (2011) investigated the right parietal cortex, including the IPCC, using mixed anatomical criteria: Areas had to be both compact and similarly connected as measured with diffusion MRI. An ROI that included the anterior parts of the occipital lobe and the parietal operculum was subdivided into 5 areas, arranged along the rostral-caudal axis. Additionally, they investigated functional connectivity from parietal cortex to some frontal and medio-temporal target areas using functional magnetic resonance imaging (fMRI) resting-state activity in both macaque monkeys and humans.

If human and macaque IPCC are indeed homologous brain regions, their long-range connectivity (The term "long-range connectivity" here refers to fiber connections that run through the white matter, as opposed to "short-range" intracortical connections.) patterns should be similar. This has been demonstrated recently by Caspers et al. (2011), who compared tract-tracing results from macaques with probabilistic tractograms of cytoarchitectonically predefined areas in humans.

Here, in contrast to the work of Caspers et al. (2011), we used dMRI probabilistic tractography, not only to characterize the connectivity profiles of IPCC subareas, but also to define these subareas in the first place. In extension to the work of Mars et al. (2011), we aimed at studying interhemispherical differences and similarities in IPCC structural organization in the light of the known strong functional lateralization (see

above), at directly comparing the anatomical parcellation and connectivity of IPCC with the connectional architecture of macaque IPCC (based on classical tract tracing), and at assessing the interindividual variance of the parcellation results and the associated connectivity patterns. The results will help to resolve the question of whether or not there is a fine-grained homology between human and macaque IPCC.

## Materials and Methods

### Participants

Twenty right-handed volunteers (10 males and 10 females, age  $25.5 \pm 3.5$  years) participated in the study. All participants gave written informed consent before being included in the experiment. The participants had no history of neurologic, psychiatric, or other major medical disorders and did not take any medication at the time of data acquisition. The experimental set-up was approved by the local ethics committee of the University of Leipzig, Germany. Data were handled anonymously.

### Data Acquisition and Preprocessing

We acquired diffusion-weighted and high-resolution 3-dimensional (3D)  $T_1$ -weighted images on a Siemens 3-T Trio scanner with an 8-channel array head coil and maximum gradient strength of 40 mT/m. For the dMRIs, we employed a spin-echo echo-planar imaging sequence (repetition time, TR = 12 s, echo time, TE = 100 ms, 72 axial slices, resolution  $1.7 \times 1.7 \times 1.7$  mm, no cardiac gating, 60 diffusion directions evenly distributed over the hemisphere,  $b$ -value =  $1000 \text{ s/mm}^2$ ). In addition, we acquired 7 data sets with no diffusion weighting, first at the beginning and then after each block of 10 diffusion-weighted images, to serve as anatomical reference for motion correction. To increase the signal-to-noise ratio, we repeated the measurement 3 times, resulting in a total scan time of approximately 45 min. For the high-resolution  $T_1$ -weighted images, we employed a 3D magnetization-prepared rapid acquisition with gradient echo sequence (TR = 1300 ms, time to inversion = 650 ms, TE = 3.97 ms, flip angle  $10^\circ$ , 176 sagittal slices, resolution  $1.0 \times 1.0 \times 1.0$  mm, 2 repetitions, total scan time 12 min).

We reoriented the  $T_1$ -weighted images to the sagittal plane through the anterior and posterior commissures and used the images without diffusion weighting to estimate motion correction parameters using rigid-body transformations (Jenkinson et al. 2002), implemented in FSL (<http://www.fmrib.ox.ac.uk/fsl>; FMRIB Software Library, University of Oxford). We combined the motion correction for dMRI data with global registration to the  $T_1$  anatomy, corrected the gradient directions of each volume with the rotation parameters, interpolated the registered images to an isotropic voxel resolution of 1 mm, and averaged each subject's 3 acquisitions. Finally, we computed the diffusion tensor, the 3 eigenvectors, and the fractional anisotropy (FA) value for each voxel (Basser et al. 1994). The FA image was used to create a mask for the tractography, including brain white matter and neighboring gray matter (threshold: FA > 0.08). By rigid mapping of the diffusion images and the gradient directions to the standardized anatomical space, we were able to perform tractography in a common anatomical space. The rigid registration of all dMRIs to the slightly rotated  $T_1$  space introduces the same amount of smoothing (caused by the interpolation) to all dMRIs. This reduces a potential directional bias, which might be caused by a varying amount of interpolation for the different dMRIs in the motion correction procedure. Additionally, the registration to the  $T_1$  space circumvented additional alignment steps after the preprocessing, without altering the tractography results compared with a tracking procedure in the native diffusion space. This was confirmed by computing the cross-correlation between the tractograms computed in the 2 different spaces, quantified by a high correlation value (mean correlation in a single ROI = 0.85, SD 0.02).

### Definition of the Region of Interest

Initially, the ROIs for tractography and parcellation were manually defined simultaneously on the pial and inflated white matter surfaces (Fischl et al. 1999) as generated by FreeSurfer (<http://surfer.nmr.mgh>).

[harvard.edu](http://harvard.edu); Martinos Center for Biomedical Imaging, Boston, USA). Since we focused our analysis on the convexity of the inferior parietal cortex, we excluded areas lying in the depth of the intraparietal sulcus (IPS), postcentral sulcus, and parietal operculum. Hence, we chose macroanatomical landmarks on or close to the exposed cortical surface as borders of the ROI: The lateral lip of the IPS (1 in Fig. 1A), the caudal lip of the postcentral sulcus (2 in Fig. 1A), the dorsal lip of the lateral fissure (3 in Fig. 1A), and the caudal shoulder of the angular gyrus (4 in Fig. 1A). The neighboring 2 cytoarchitectonically and functional different areas called the human intraparietal area 1 and the human intraparietal area 2, in the IPS ([Choi et al. 2006](#)), which extend up to the shoulder of the sulcus were assured not to be part of the ROI. For the correct identification of the sulci, we used the “Atlas of the Cerebral Sulci” ([Ono et al. 1990](#)) to analyze the sulcal variability.

As a second step, we transformed the defined surface labels into the voxel space and used them as template to interactively mark all voxels within this ROI that are located at the gray-white matter interface (derived from the coregistered FA images with  $FA > 0.15$ ) using the software Anatomist (<http://anatomist.info>, Service Hospitalier Frédéric Joliot, CEA, Orsay, France) (1 in Fig. 1B). These voxels were used as seed points for subsequent diffusion tractography (2 in Fig. 1B). Voxels in the fundus of the bordering sulci were excluded to prevent connections with deep white matter structures in the parietal lobe like the long segment of the arcuate fascicle ([Catani et al. 2005](#)).

#### Tractography and Connectivity-Based Parcellation

We used the probabilistic tractography method and the connectivity-based parcellation scheme similar to the one proposed by [Anwander et al. \(2007\)](#). The underlying concept of connectivity-based parcellation is that cortical areas with similar anatomical connectivity are combined into a region, which is segregated from neighboring regions with different connectivities. The connectivity pattern of a cortical voxel is approximated by the tractogram associated with its immediately underlying white matter voxel. Figure 1B illustrates the general principle of the parcellation technique. For each seed voxel within the ROI (1 in Fig. 1B), we computed a probabilistic tractogram (2 in Fig. 1B) and arranged the correlation values between any 2 of these tractograms in a connectivity correlation matrix. In contrast to [Anwander et al. \(2007\)](#), who used a *k*-means clustering approach in order to define the groups

of voxels with similar connectivity (3 in Fig. 1B), we applied a cluster algorithm based on a Gaussian Mixture Model (as implemented in MatLab<sup>TM</sup>) to the columns of the connectivity correlation matrix. This technique is better suited to cope with clusters, showing differences in intracluster homogeneity ([Gorbach et al. 2011](#)).

A challenge for any clustering method is the trade-off between model consistency (how well does the clustering describe the structure of the data) and model complexity (preference of a simple model that describes the relevant features and ignores noise). Here, the clusters had to be defined *a priori*. We tested the different numbers of clusters ( $2 \leq n \leq 7$ ), but accepted only those solutions that were consistent across hemispheres and participants, that is, the principal arrangement of cortical areas (e.g., from inferior to superior or from anterior to posterior) associated with the clusters had to be the same. As a second requirement, each area had to represent a single topologically compact region of the cortex. Additionally, we characterized each area by its tractographic signature (i.e. its average tractogram). As a final step, we mapped the resulting clusters back onto the cortical surface of each individual brain (4 in Fig. 1B). The fact that this clustering approach yields neuroanatomically meaningful results has been substantiated in recent publications ([Johansen-Berg et al. 2005](#), [Anwander et al. 2007](#), [Beckmann et al. 2009](#), [Schubotz et al. 2010](#)).

For interpretation of the parcellation results, we first assessed the positions (computed as center-of-mass, in Talairach coordinates) and sizes (by voxel counting) of all IPCC subareas in all participants and hemispheres. We computed the mean and standard deviation (SD) of these values for all participants.

To assess each area's topographical variability, we computed for each cluster a population overlap map. Therefore, we dilated the clusters (voxels at the gray-white matter interface) by 3 mm orthogonally to the surface and normalized all individual brains and clusters to the Montreal Neurological Institute (MNI) single-subject brain (known as “colin27”), superimposed them in 3D space, and computed the population maps (Fig. 5). This map shows, for each cluster and each voxel in MNI space, how many brains ( $0 \leq n \leq 20$ ) have a representation of this cluster in the particular voxel.

#### Connectivity Analysis

We qualitatively assessed the global connectivity profile of each IPCC subarea by mapping the values of its tractographic signature. The

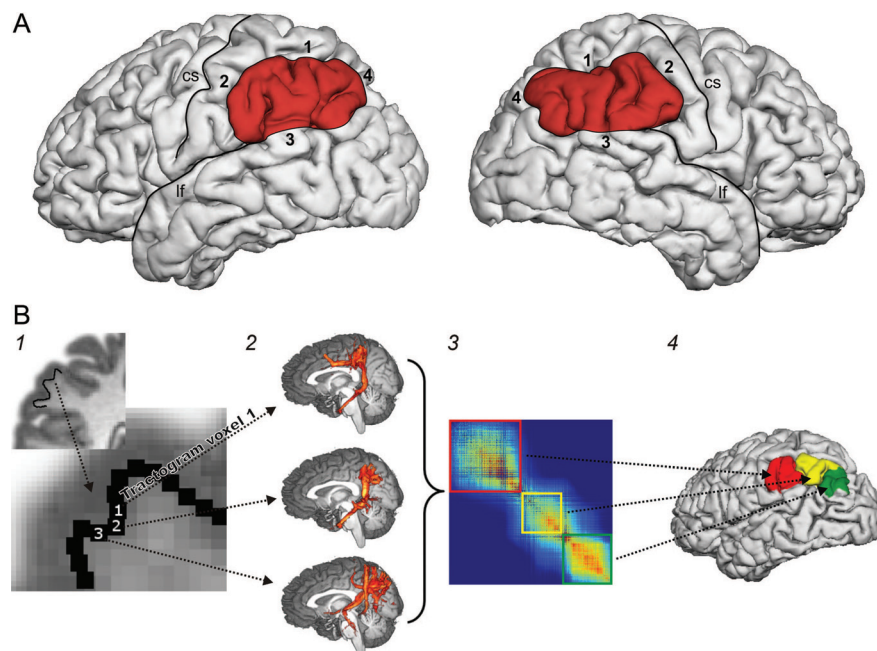


**Figure 1.** (A) Inferior parietal cortex ROI on a representative subject. (1) IPS/lateral lip; (2) postcentral sulcus/caudal lip; (3) lateral fissure/dorsal lip; (4) angular gyrus/caudal shoulder; cs, central sulcus; If, lateral fissure. (B) General methodology of connectivity-based cortex parcellation. (1) Seed voxels for probabilistic tractography are placed in white matter at the gray-white matter interface of the IPCC. (2) For each of these voxels, a probabilistic tractogram is computed. (3) The matrix containing the correlations between all these tractograms is divided into clusters of voxels with similar correlation to the tractograms of other voxels. (4) Each of these clusters corresponds to a certain area on the cortical surface.

seed regions for the tractography were derived from the population map with a minimum overlap of 5 participants. Seed voxels within overlapping areas were assigned to the subarea with the maximum probability value. For tractography, the seed regions were morphed to the single-subject brains. The connectivity was computed using a total of 100 000 random walks (cf. Anwander et al. 2007) per seed region. The single-subject connectivity patterns were normalized to the MNI brain and averaged over all participants. The average connectivity values in the gray-white matter interface were visualized on an inflated cortex representation of the MNI brain (Fig. 6). To quantitatively compare the connectivity patterns between the subareas, and thereby establish significant differences between these areas in terms of long-range connectivity, we analyzed each area's connectivity strength with specific target regions for all participants separately. For this purpose, we interactively defined 10 gyrus-based target ROIs (on the average brain over 20 participants; see Fig. 2).

These target ROIs were defined by macroanatomical landmarks (sulci) on the inflated brain surface by manual refinement of the automatic gyrus labeling computed by FreeSurfer (Martinos Center for Biomedical Imaging). The labeled cortical regions were mapped onto the brain volume and warped by nonlinear registration of the mean brain to the individual  $T_1$  anatomy of the 20 participants. The correct warping of the target regions were manually validated in every individual subject. Analog to the seed ROI definition, we labeled all voxels at the gray-white matter interface within each region as target voxels. On a single participant basis (and separately for each hemisphere), we computed how many of the random walks starting in each IPCC subarea reached each target. For statistical analysis of these connectivity values, which cannot be assumed to follow a normal distribution, we used the nonparametric Friedman repeated-measures analysis of variance model (factor 1: IPCC area, factor 2: target; each hemisphere treated separately) and a Wilcoxon signed-rank test for post hoc pairwise comparisons between the levels of factor 1 (i.e., IPCC areas). All  $P$ -values were Bonferroni corrected for multiple comparisons. For testing connectivity differences between the hemispheres, the same procedure was used.

## Results

We varied the number of clusters between 2 and 7 and found 3 to be the maximum number, for which the clusters were compact with a consistent principal spatial arrangement across

participants (see Materials and Methods). More specifically, in 37 of the 40 tested hemispheres, we found 3 compact, and approximately equal-sized regions, in a roughly rostral-caudal arrangement, referred to as inferior parietal cortex anterior (IPCa), IPC middle (IPCm), and IPC posterior (IPCp; Fig. 3). Figure 3 also shows the morphometric characterization of the areas in 4 typical participants (for all participants, see Supplementary Fig. 1a,b in the Supplementary data).

The variability and reproducibility of the parcellation results of all participants are represented by the centers of mass of subareas (Fig. 4). From Figure 4, one can see that IPCa mainly coincides with the supramarginal gyrus (roughly BA 40), while IPCp maps onto the angular gyrus (BA 39). Area IPCm is located in the transition area between the 2 gyri. The IPCCs of the left and right hemispheres (as well as the corresponding subareas) were found to have similar sizes (Fig. 4). Comparing the sizes of the subareas across hemispheres, we found similar sized IPCm and IPCp and a slightly bigger IPCa. The size of the subareas was measured by counting the number of boundary voxels at the gray-white matter interface. This number was converted into  $\text{cm}^2$  representing the size of each areas folded surface. The centers of mass of the subareas show a consistent rostro-caudal arrangement across participants. In the right hemisphere, the regions are located slightly more anteriorly. The variability of the spatial location across participants is comparable for all subareas (see SDs in Fig. 4).

Figure 5 shows the population maps, illustrating that the variability of the computed IPCC subareas over participants displayed on the single-subject MNI standard brain. The strong overlap of the population map across subjects shows the consistency of the subdivision into 3 areas. The agreement was best for the IPCa area. Left and right hemispheres show similar results. The full 3D population maps in the MNI space of all IPCC areas are publicly available (<http://opencolor.cbs.mpg.de/ipcc>) and additionally provided in Supplementary data (Supplementary file 3), which can be used with functional imaging software packages, such as FSLView or SPM.

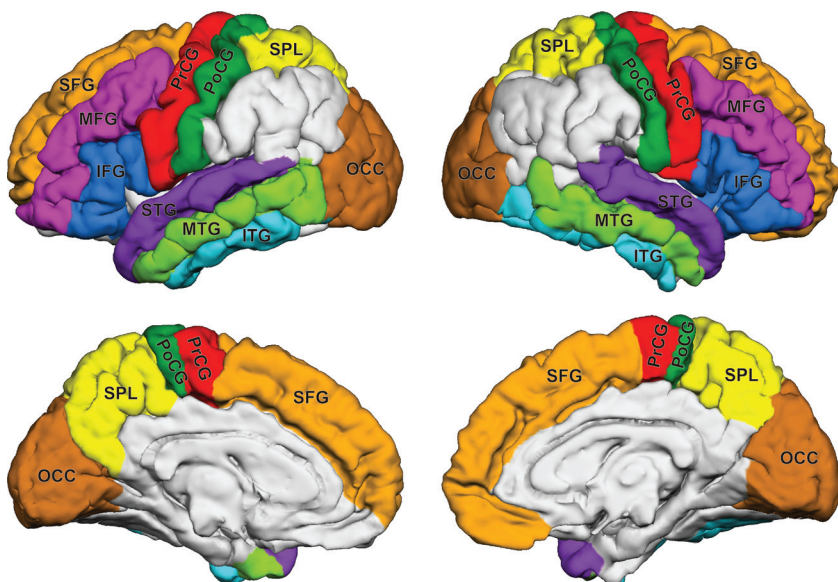


**Figure 2.** Gyrus-based target ROIs superimposed on the mean brain of all 20 participants in the MNI space. SFG, superior frontal gyrus; MFG, middle frontal gyrus; IFG, inferior frontal gyrus; PrCG, precentral gyrus; PoCG, postcentral gyrus; SPL, superior parietal lobe; STG, superior temporal gyrus; MTG, middle temporal gyrus; ITG, inferior temporal gyrus; OCC, occipital lobe.

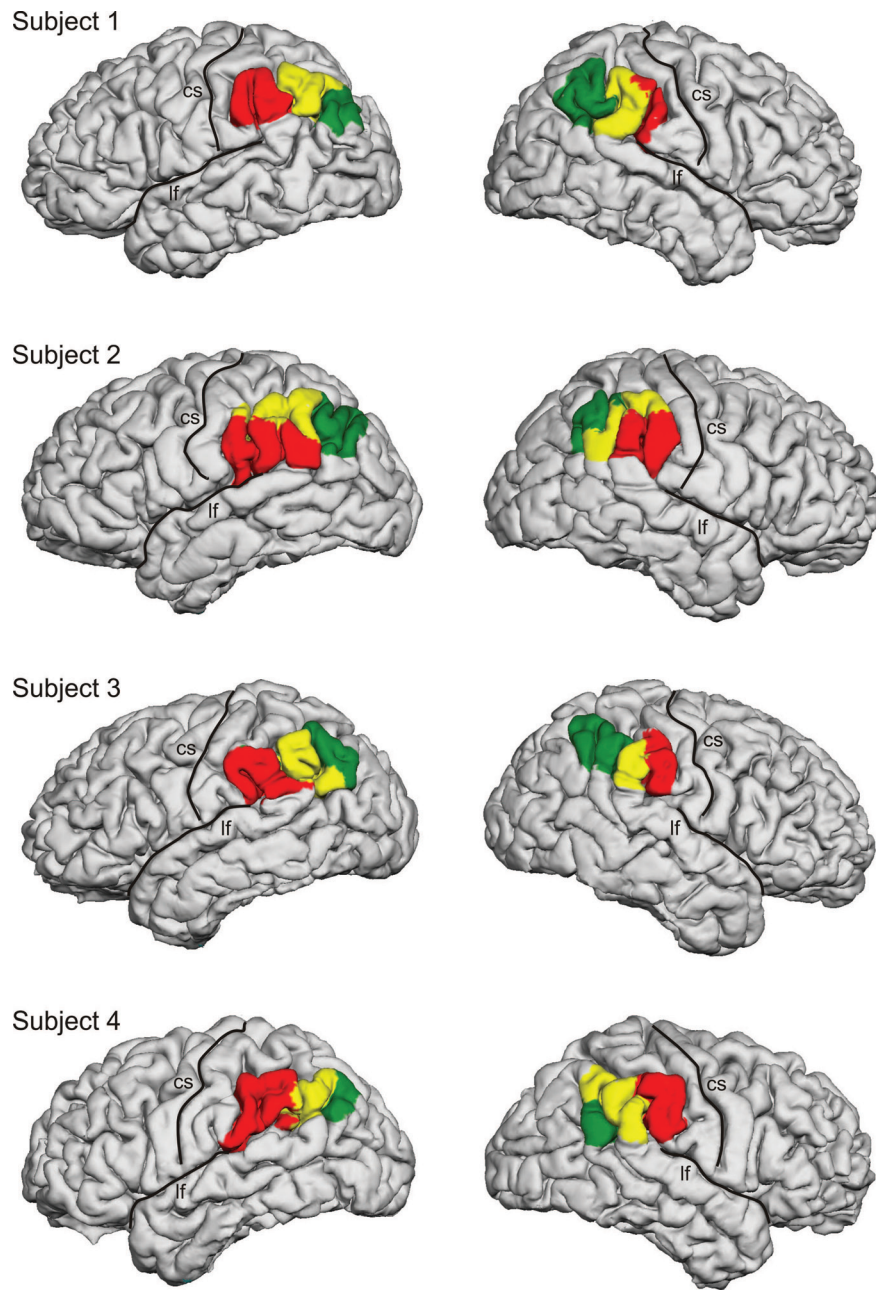


**Figure 3.** Parcellations of the left and right IPCC of 4 representative participants into IPCCa (red), IPCm (yellow), and IPCp (green) superimposed on a 3D reconstruction of the pial surface; cs, central sulcus; lf, lateral fissure.

Figure 6 shows, for each IPCC subarea, the group average of the connectivity, as quantified by the tractographic signature value in the gray-white matter interface. This representation provides a high-resolution overview on the connectivity profiles of the areas. The connectivity patterns show a strong overlap between areas, but there are also some substantial differences. For example, connections to the ventral premotor cortex are stronger for anterior when compared with posterior regions, and connections to the temporal lobe are stronger in the left hemisphere than that in the right. This illustration of the mean tractogram on the inflated brain surface (Fig. 6) allows a precise localization of areas connected to the IPCC. Beside local connections to the neighboring parietal and temporal areas, all IPCC areas show a long-range connection to

the precentral gyrus (PrCG) via the superior longitudinal fascicle (SLF). Additionally, a ventral connection to the anterior inferior frontal gyrus (IFG) via the extreme capsule fiber bundle was found for the left IPCp. A slice view of the fiber bundle showing the precise location of the connections within the white matter is provided in Supplementary data (Supplementary Fig. 2).

The connection strengths between the IPCC subareas and the cortical target regions are depicted in Figure 7A. Table 1 summarizes the results of the statistical tests. The strongest connections of the areas IPCCa, IPCm, and IPCp were found to the lateral temporal cortex (superior temporal gyrus, STG; middle temporal gyrus, MTG; and inferior temporal gyrus, ITG), the SPL, the pre- and postcentral gyri (PrCG and PoCG),

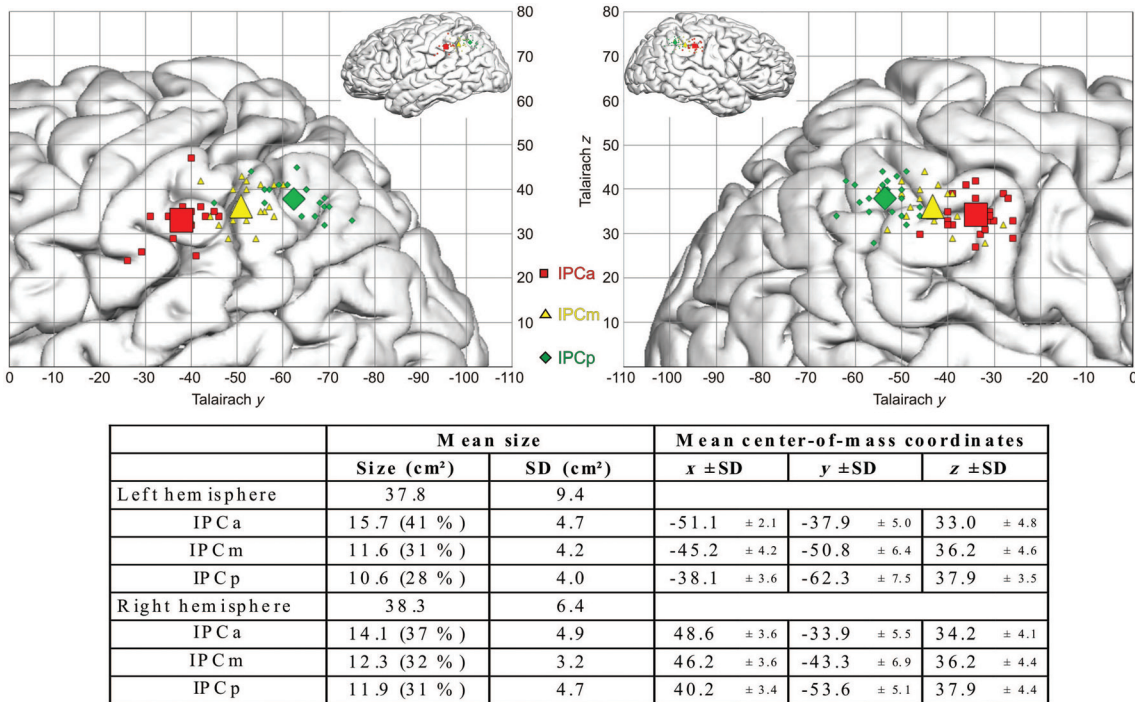


**Figure 4.** Top: Illustrating the centers of mass of IPCa (red), IPCm (yellow), and IPCp (green) in the left (left) and right (right) hemispheres superimposed on the Talairach coordinate system. Small symbols represent the center of mass of each individual subject, and large symbols are the mean center of mass across all participants. Bottom: Size (in cm<sup>2</sup>) and locations (in Talairach coordinates) of the different IPC subareas.

and the ventro-lateral prefrontal cortex (IFG and middle frontal gyrus, MFG; only in the right hemisphere). Connections with the occipital cortex, the dorso-lateral prefrontal cortex (in both hemispheres), and the ventro-lateral prefrontal cortex (in the left hemisphere) are weaker. There is a significant rostro-caudal (i.e., IPCa-to-IPCp) decrease in connectivity strength to the superior temporal and inferior frontal cortex in the right hemisphere. Moreover, we identified a similar rostral-caudal decrease in connectivity to the superior temporal cortex, and an increase in connectivity to the superior parietal cortex in the left hemisphere (Fig. 7A).

In the left hemisphere, we found strong connections to both the lateral temporal cortex and the superior parietal cortex and weaker connections to both the occipital cortex and the lateral frontal cortex. The right hemisphere shows strongest connections to the lateral temporal cortex, superior parietal cortex, and lateral frontal cortex. Only sparse connectivity exists to the occipital cortex. Additionally, both hemispheres show relatively strong connectivity to the pre- and postcentral gyri.

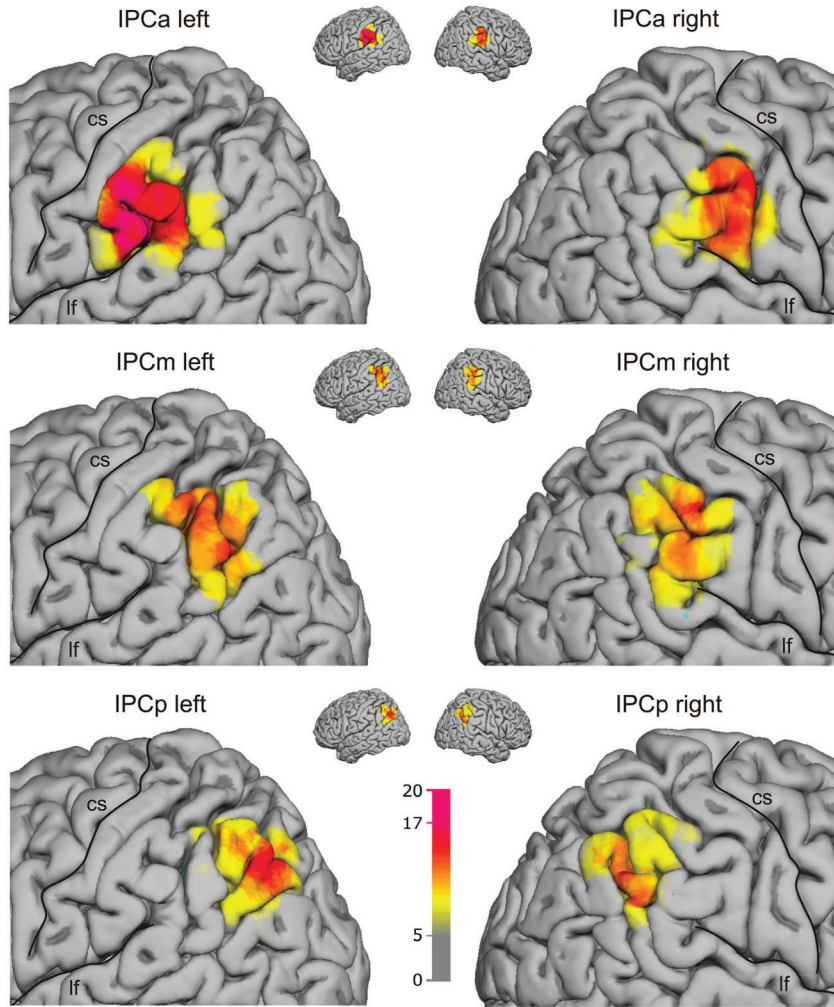
To test for significance, we performed a 2-way repeated-measures Friedmann analysis of variance on ranks (factor 1: IPC region and factor 2: target region), followed by a Wilcoxon signed-rank test for post hoc pairwise comparisons. The test results show significant differences between IPCa, IPCm, and IPCp in their connectivity strength to both the superior temporal cortex and superior parietal cortex. In the right hemisphere, significant differences were also found in the connection strength to the superior temporal cortex and furthermore to the inferior frontal cortex (Fig. 7A and Table 1).

Figure 7B shows the comparison between the connectivity patterns of the corresponding areas in the 2 hemispheres. In

IPCa, the left area has more connections to the MTG, while the right area connects stronger to the STG, SFG, and IFG. For the middle area IPCm, the right side has stronger connections to the SFG and IFG. Finally, IPCp shows a stronger right-side connectivity for the PrCG.

## Discussion

In this study, we show that the human IPCC can be divided into 3 subareas, arranged in a rostral-caudal direction, with distinct connectivity patterns to the rest of the brain. In addition, the principal topological arrangement and the connectivity patterns of these subareas are relatively consistent across participants. The variability between subjects is comparable for all regions and both hemispheres (Fig. 4). Moreover, the connectivity patterns are in principal agreement with previous dMRI-based studies of the parietal lobe. For example, connections between rostral IPCC and IFG, as well as ventral premotor and somatosensory areas, have been demonstrated by Rushworth et al. (2006), Mars et al. (2011), and Caspers et al. (2011). While we consistently found for all subareas strongest connections to the lateral temporal and superior parietal cortices, there were also striking differences between subareas: A rostral-caudal decrease in connection strength to the inferior frontal (only for the right hemisphere) and superior temporal regions (both hemispheres), and a rostral-caudal increase in connection strength to the superior parietal cortex (only for the left hemisphere). Note that it could be argued that the rostral-caudal decreases in connectivity are due to the distance bias associated with probabilistic tractography (Jones 2010). However, as can be seen in Figure 7A,B, the decrease in IFG connectivity from IPCa to



**Figure 5.** Population maps ( $n = 20$  brains, cf. color bar) of areas IPCa (top), IPCm (middle), and IPCp (bottom) superimposed on the MNI single-subject brain; cs, central sulcus; lf, lateral fissure. Voxels that belong to the respective area in <5 participants are not shown.

IPCP amounts to about a factor between 3 and 5. The upper bound of the distance bias (if fibers spread completely uniformly into all directions) in probabilistic tractography is proportional to the square of the distance. If the diffusion is constrained by coherent structure, this exponent is much lower. Simulations show that it is in the order of 1, which has been used, for example, by Greenberg et al. (2012) and Anwander et al. (2007). As the distance from IFG to IPCP is less than twice the one from IFG to IPCa (Fig. 8), the difference in connection strength cannot be purely an effect of distance bias.

#### What is the Most Appropriate Subdivision of the IPCC?

As with other cortical areas, the exact subdivision of human IPCC has been a matter of debate. For example, Brodmann (1909), on the basis of postmortem cytoarchitectonics, postulated a subdivision into 2 areas, while later researchers, even when using the same principal methodology, concluded that there should be a higher number of subareas (von Economo and Koskinas 1925; Gerhardt 1940; Sarkissov et al. 1955; Caspers et al. 2006). Recently Caspers et al. (2013) used receptor mapping to suggest that the 7 cytoarchitectonically defined IPCC subareas (Caspers et al. 2006) can be clustered into 3 larger rostro-caudally arranged regions. Moreover,

using postmortem myeloarchitecture as a structural criterion leads to more than 2 subareas of IPCC (Vogt 1911; Batsch 1956).

The rostral-caudal arrangement found in this study is in agreement with a number of previous studies using cytoarchitectonics (e.g., von Economo and Koskinas 1925; Sarkissov et al. 1955; Caspers et al. 2006) and dMRI connectivity (Mars et al. 2011). Concerning the number of distinguishable areas, however, there are differences. Mars et al. (2011) subdivided, at least, the right IPCC into 5 rostro-caudally arranged areas, consistently over several participants. Here, we must consider 2 facts. First, these authors used a large ROI that included both the parietal operculum (indeed, 1 of the 5 clusters was mainly located there) and anterior parts of the occipital lobe. Secondly, Mars and colleagues did not only rely on anatomical connectivity for parcellation, but additionally asked for compact clusters. This additional assumption might have stabilized the parcellation and allowed for a higher number of subareas to be consistent across participants. Caspers et al. (2006) found 7 cytoarchitectonically defined rostro-caudally arranged areas altogether. However, they also acknowledge that neighboring areas tend to be similar and can be combined (cytoarchitectonic gradient).

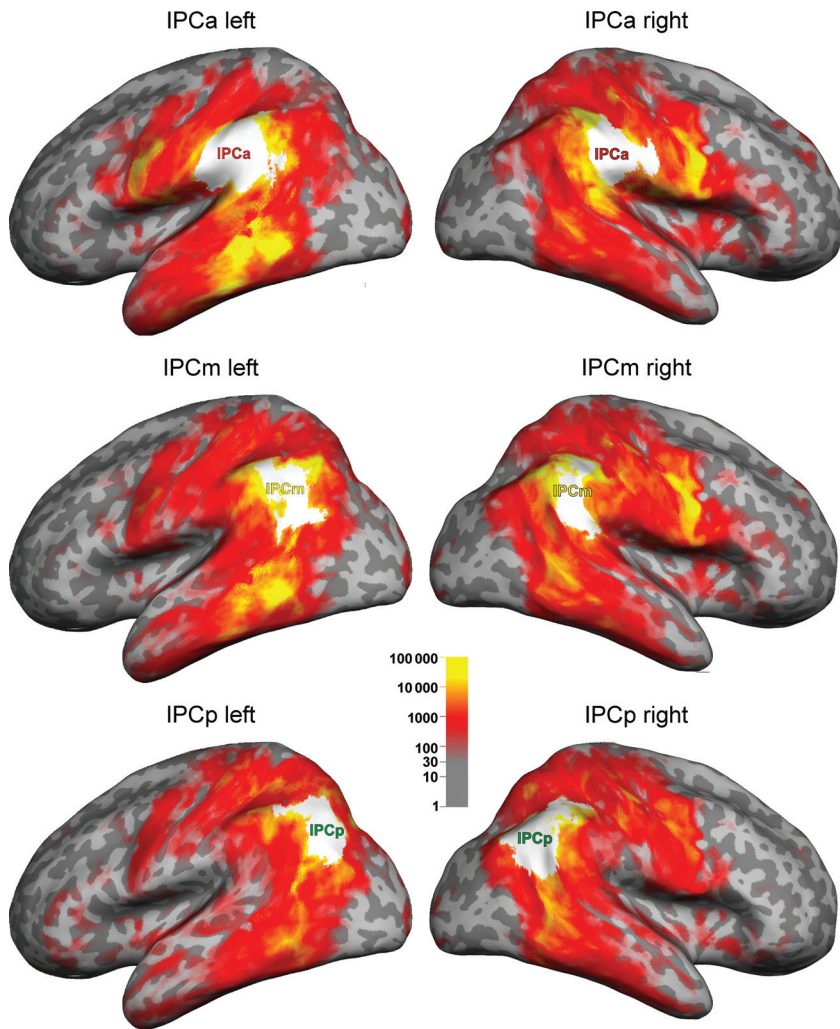


**Figure 6.** Group-averaged connectivity of the IPCC subareas displayed on an inflated MNI brain. The white areas characterize the average seed areas and are derived from the population maps (Fig. 5) with a minimum of 5 participants (no overlap between seed regions).

So, it seems that the anatomical similarity structure of the cortex across studies in the field does not converge to a clear distinction into a fixed number of homogeneous and clearly distinguishable areas. Instead, it appears that the number, location, and precise boundaries of areas are a matter of: (1) The structural traits used as parcellation criteria (e.g., cytoarchitecture or long-range connectivity) and the sensitivity of the methodology to extract them, and (2) the level of detail considered relevant for the particular researchers (i.e., the desired granularity of the parcellation). With respect to the former point, one may conclude that an exact agreement between the earlier results based on cortical microstructure and our findings based on long-range connectivity profiles is neither necessary nor likely. Concerning the latter point, the question remains: How many subareas of the IPCC would represent the most appropriate parcellation? Here, we argue that it is sensible to choose the most detailed description (i.e., the largest number of areas) that still leads to a consistent pattern across participants. Any attempt to produce finer parcellations would highlight interindividual differences, while any coarser subdivision would miss potentially relevant features. The remaining variability of cluster size and location might be a

source to study the individual arrangement of functional zones in the IPC. Based on these considerations, the criterion of long-range connectedness and using the current technology to characterize this connectedness, we suggest that a subdivision of the IPCC into 3 areas is the most appropriate.

#### **Connectivity Pattern of the Human IPCC**

This study shows strongest connections of the IPCC to the lateral temporal, superior parietal, and pre- and postcentral cortices in both hemispheres. The IPCC subareas are characterized by a significant rostral-caudal (i.e., IPCa-to-IPCp) decrease and increase in particular connectivity patterns to certain cortical areas. A connectivity decrease from rostral to caudal was identified to the superior temporal cortex in both hemispheres, and an increase to the superior parietal cortex in the left hemisphere.

In agreement with the study from Caspers et al. (2011), we identified the strongest connections between all IPCC subareas and the temporal cortex. We also found a comparable connectivity pattern in the left and right hemispheres. On the other hand, some of the rostral-caudal connectivity gradients

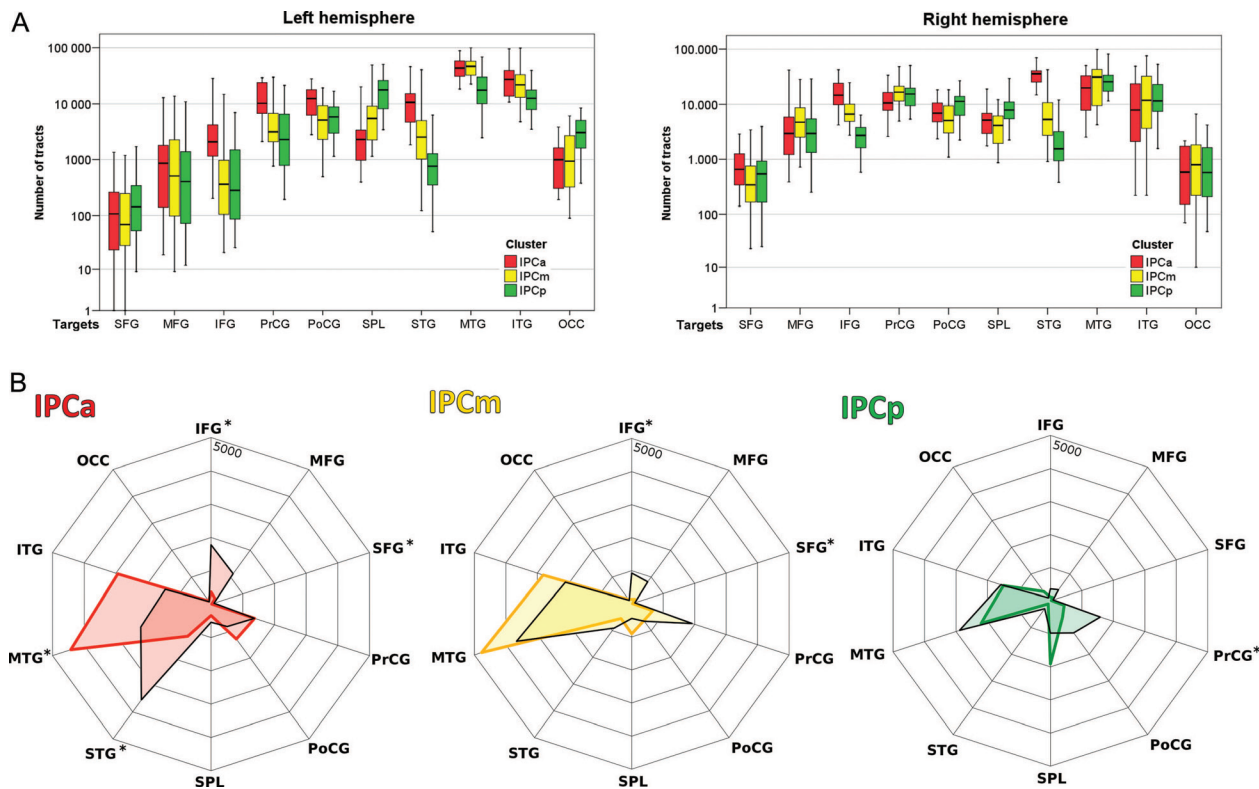


**Figure 7.** (A) Connectivity between the areas IPCa, IPCm, and IPCp and the cortical target regions ( $n = 20$  participants). The box-and-whisker diagrams show the median values, the lower and upper quartiles (boxes), and upper and lower bound (whiskers). (B) Statistical comparison of connectivity fingerprints of IPCC subareas between hemispheres. The mean values are indicated by colored lines for the left areas and black lines for the right areas. An asterisk marks those connections that are significantly different between the hemispheres ( $P < 0.01$ , based on the Wilcoxon test; see Materials and Methods for details).

of the current work differ from the study of Caspers and colleagues, in which, for example, rostral areas are more connected to somatosensory and superior parietal areas, while caudal areas are predominantly connected to the auditory, anterior temporal and occipital cortex. The connections patterns are not directly comparable due to differences in the methodology to compute the connectivity values from diffusion tractography. However, the main difference consists in the definition of seed and target regions. While we used the voxels at the gray-white matter interface in the entire IPCC subareas as seed region, Caspers et al. (2008) used a small area representing the top 10% of the maximum probability map and computed the connectivity values to a small target zones within the target areas. Further on, their measures are based on the connection likelihood and not on the connection strength computed by probabilistic tractography.

#### Methodological Considerations

The measured diffusion signal is only an indirect measure of the brain microstructure and, therefore, the derived tractography does not directly reflect the fine details of anatomical connectivity (Jones et al. 2013). Some of the computed connections might not exist in the brain (false-positive connections) and the method cannot capture the full connectivity of the brain (false-negative connections). The estimated connectivity values do not represent the true axonal fiber-count in the living brain and are only a relative measure of linkage between regions. Nevertheless, the computed estimation of the long-range connectivity is a powerful criterion to separate cortical areas with different

connectivities, even if definite connectivity remains unknown. Despite these limitations, diffusion tractography provides relevant information of the white matter connectivity as shown in numerous studies (e.g. Assaf and Pasternak 2008).

#### Homology—Comparison with Monkey data

Besides having optimal consistency across participants, the proposed subdivision of human IPCC into 3 subareas arranged in rostral-caudal direction is also supported by its similarity to the subdivision of the macaque IPCC (areas PF, PFG, and PG), according to studies of cytoarchitecture (Gregoriou et al. 2006), tract tracing (Rozzi et al. 2006), and electrophysiology (Rozzi et al. 2008). The small area Opt, the fourth area in the macaque IPCC, which is located on the boundary to the occipital lobe markedly differs from the other IPCC areas in terms of cytoarchitecture and connectivity (Pandya and Seltzer 1982; Rozzi et al. 2006) and is not clearly associated with the parietal lobe. We therefore excluded this area from the comparative analysis.

The next question is whether the human and the macaque areas are comparable with respect to their connectivity patterns, and whether there are any important differences between the 2 species. In the macaque, areas PF, PFG, and PG are connected with the lateral premotor cortex (areas F4 and F5) and the intraparietal and superior parietal cortices via the SLF II/III (Rozzi et al. 2006; Schmahmann and Pandya 2006). Similarly, in humans, the areas IPCa, IPCm, and IPCp are connected with the IFG (containing BA 44, the presumed human homolog of macaque area F5) and the superior

**Table 1**

Test results for differences between the connection strength of IPCC subareas

	SFG	MFG	IFG	PrCG	PoCG	SPL	STG	MTG	ITG	OCC
Left hemisphere										
Friedmann	***	***	***	***	***	***	***	*	***	
Wilcoxon										
IPCa-IPCm	***	***	***	**	***					
IPCa-IPCp	**	***	***	***	***	**	**	**	***	
IPCm-IPCp	(*)			**	***	**	*	*	***	
Right hemisphere										
Friedmann	***			**	***					
Wilcoxon										
IPCa-IPCm	**					***				
IPCa-IPCp	***			*	***					
IPCm-IPCp	***			***	***					

Note: Levels of significance: (\*)  $P < 0.1$  (marginally significant), \* $P < 0.05$ , \*\* $P < 0.01$ , \*\*\* $P < 0.001$ . The  $P$ -values are Bonferroni corrected for multiple comparisons. See text for details and legend of Figure 2 for the regions and abbreviations.

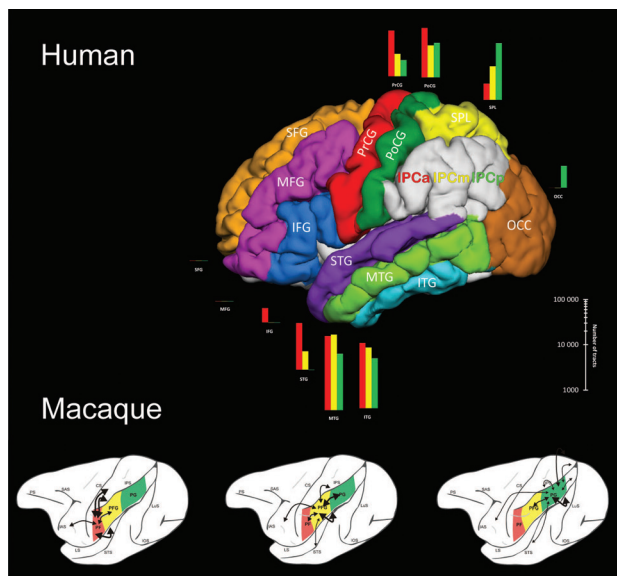


**Figure 8.** Parcellation and connectivity strengths of IPCCa (red), IPCm (yellow), and IPCp (green) with other regions in humans (top), compared with PF, PFG, and PG in macaque (bottom) ("classical" tract-tracing data in the macaque from [Rozzi et al. 2006](#)).

parietal cortex. These similarities in parieto-frontal connections are also corroborated in a recent study by [Thiebaut de Schotten et al. \(2011\)](#), who demonstrated a striking similarity between the architecture of the SLF in both macaques and humans.

In addition to these similarities, there are also clear differences (Fig. 8). In monkeys, only sparse connections seem to exist between the IPCC and the temporal cortex (see [Seltzer and Pandya 1984](#); Fig. 8; [Rozzi et al. 2006](#); [Schmahmann et al. 2007](#)). In marked contrast to that, in humans, strong connections exist between all 3 regions of the IPCC and the lateral temporal cortex. These connections follow the posterior, vertical section of the arcuate fascicle ([Catani et al. 2005](#)). [Connections to deep white matter structures (e.g., the long segment of the arcuate fascicle) were excluded by carefully selecting the seed region at the cortical interface (see Materials and Methods).] Additionally, tractography revealed strong connectivity of all 3 regions with the pre- and postcentral gyri. These connections were not described in this extend in the macaque monkey.

The similarity in IPCC parcellation between macaques and humans and the similar connections between the IPCC and frontal and parietal regions suggest substantial conservation in IPCC evolution between the 2 primate species. However, in humans, new structural features emerged, such as the pronounced pathway between the IPCC and temporal cortex, which is possibly part of a perisylvian language network of the human brain ([Catani et al. 2005](#); [Schmahmann et al. 2007](#); [Friederici 2009](#)).

### The Functional Relevance of the IPCC Parcellation

As discussed in the Introduction, subareas of the IPCC are involved in several important cognitive networks, including those subserving language, spatial attention, and episodic memory. These networks have been investigated in numerous functional brain imaging studies. We will now discuss how the subareas we have found on the basis of tractography, as well as the associated connectional fingerprints, might relate to these functional findings. Similar to [Caspers et al. \(2006\)](#), we consider IPCm to be a transition area between the rostral (IPCa) and caudal (IPCp) subregions of the IPCC, and IPCa and IPCp as transition area to other cortical regions.

#### Rostral IPCC

The subarea IPCa covers the rostral part of the IPCC and largely corresponds to the supramarginal gyrus. This area has been interpreted to be involved in phonological processing ([Obleser et al. 2006](#)) and, together with the dorsal part of the IFG, in phonological working memory ([Vigneau et al. 2006](#)). Similarly, the area was found active for phonology–orthography mapping ([Graves et al. 2010](#)), phonological decision ([Hartwigsen et al. 2010](#)), and subvocal articulation ([Price 2010](#)). This phonological network comprises, besides bilateral IPCCa and the IFG, posterior MTG and fusiform gyrus ([Graves et al. 2010](#)). In contrast to these phonological findings, other language functions seem to markedly exclude rostral IPCC ([Vigneau et al. 2006](#)).

Furthermore, although lesions in the posterior parietal cortex do not usually cause gross memory deficits, imaging studies have shown that the region is involved in episodic memory ([Cabeza et al. 2008](#)). In particular, familiarity-based episodic memory effects are primarily found in the supramarginal gyrus ([Vilberg and Rugg 2008](#)).

Finally, rostral IPCC seems to store abstract somatosensory information associated with tool use and complex movements ([Binder et al. 2009](#)). Hence, it should be in close connection with other motor and somatosensory areas, such as on the pre- and postcentral gyri. Indeed, [Rizzolatti and Craighero \(2004\)](#) have shown that the rostral IPCC belongs to the mirror neuron network and is activated during imitation and observation of actions (see also [Caspers et al. 2010](#)). In these studies, it was also shown that rostral IPCC coactivates with premotor and somatosensory cortices.

Similar networks to the ones found by the experiments described above also seem to emerge from resting-state fMRI studies (e.g., [Kelly et al. 2010](#)).

In our analysis, we found substantial connections between IPCCa and all tested target regions. However, the regions most strongly connected to IPCCa comprise the IFG, pre- and postcentral gyri, as well as the temporal lobe (ITG, MTG, and STG). This network includes, but is not limited to,

functionally connected areas discussed above (note that fusiform gyrus was not tested here).

Comparing the connection strength between the hemispheres, we first find a right lateralization of connections between IPCa and prefrontal (IFG and SFG), as well as superior temporal (STG) areas. While the frontal connections fit well with a right lateralized visuo-spatial attention network (Umarova et al. 2011), the meaning of the strongly right lateralized STG and the strongly left lateralized MTG connections remains somewhat unclear.

#### Caudal IPCC

The caudal subarea of the IPCC identified in our analysis (IPCp) lies on the angular gyrus. The area has been discussed as supporting semantic processes (Humphries et al. 2007) and, together with parts of the IFG, to be involved in semantic working memory (for a review see Vigneau et al. 2006).

In studies of visuo-spatial attention, besides the dorsal attention network that subserves goal-directed attention, a ventral bottom-up attention network has been discovered that underlies the direction of attention toward salient stimuli and acts as a “circuit breaker” for the dorsal network (Corbetta and Shulman 2002). This network recruits mainly angular gyrus, as well as the posterior parts of MFG and IFG.

More generally, it seems that the caudal part of the IPCC houses neuronal populations that are involved in processes of high-level, complex and supramodal integration, such as decision-making, planning, problem solving, and sentence comprehension (Binder et al. 2009).

In our study, the subareas, IPCm and IPCp, are also principally connected to all target areas. However, some areas are particularly strongly connected, such as left SPL. This fits with the idea that this area has special involvement in networks of episodic memory and spatial attention (Corbetta and Shulman 2002; Cabeza et al. 2008). On the other hand, IPCm and IPCp are also strongly connected with temporal areas of the language network, thus corroborating their involvement in language comprehension (Vigneau et al. 2006).

Concerning the interhemispheric differences between the connections of caudal IPCC we find that in the right hemisphere, there are stronger connections to the PrCG (more posteriorly, IPCp), and to IFG/SFG (more anteriorly, IPCm). This connection pattern bears a striking resemblance to the SLF III system (see Schmahmann et al. 2007), a fiber system whose right lateralization has been shown to correlate to performance in visuospatial attention tasks (Thiebaut de Schotten et al. 2011).

#### Conclusions

Our connectivity-based tripartition of the human IPCC as well as the associated connectivity patterns are in principal agreement with previous studies, both, based on diffusion tractography and invasive methods. We extend the earlier work in several ways. First, we provide direct insights into the inter-subject variability of the parcellation. These data are also provided as an atlas in Supplementary data (Supplementary file 3). Secondly, we directly assess the lateralization of parcellation and connectivity fingerprints of the subareas. While the parcellation showed only slight interhemispheric differences, the associated connections are markedly different: In contrast to the left hemisphere, the right anterior IPCC features stronger prefrontal and superior temporal connectivities, posterior

IPCC is stronger connected to the superior parietal and prefrontal areas. Thirdly, we compare and extensively discuss the relationship between our findings in humans and previous tracing work in monkeys. While the rostro-caudal arrangement of the subareas is similar to the findings in the macaque, the connectivity patterns bear important differences, in that, humans in contrast to the monkeys have strong connections between IPCC and temporal cortex, possibly related to the human ability to process language. In summary, this study gives a more complete picture of the structure of the IPCC and provides a blueprint for similar investigations of other regions of the cortex.

#### Supplementary Material

Supplementary material can be found at: <http://www.cercor.oxfordjournals.org/>.

#### Funding

This work was supported by a University Leipzig MD grant to M.R. and the Future and Emerging Technologies (FET) project CONNECT of the European Union, under FET-Open (grant no. 238292): <http://www.brain-connect.eu>.

#### Notes

We thank Tania Douglas for valuable technical advice. *Conflict of Interest:* None declared.

#### References

- Anwander A, Tittgemeyer M, von Cramon DY, Friederici AD, Knösche TR. 2007. Connectivity-based parcellation of Broca's area. *Cereb Cortex*. 17:816–825.
- Assaf Y, Pasternak O. 2008. Diffusion tensor imaging (DTI)-based white matter mapping in brain research: a review. *J Mol Neurosci*. 34:51–61.
- Basser PJ, Mattiello J, LeBihan D. 1994. Estimation of the effective self-diffusion tensor from the NMR spin echo. *J Magn Reson B*. 103:247–254.
- Batsch E. 1956. Die myeloarchitektonische Untergliederung des Isocortex parietalis beim Menschen. *J Hirnforsch*. 2:259–270.
- Beckmann M, Johansen-Berg H, Rushworth MF. 2009. Connectivity-based parcellation of human cingulate cortex and its relation to functional specialization. *J Neurosci*. 29:1175–1190.
- Behrens TEJ, Johansen-Berg H, Woolrich MW, Smith SM, Wheeler-Kingshott CAM, Boulby PA, Barker GJ, Sillery EL, Sheehan K, Ciccarelli O et al. 2003. Non-invasive mapping of connections between human thalamus and cortex using diffusion imaging. *Nat Neurosci*. 6:750–757.
- Binder JR, Desai RH, Graves WW, Conant LL. 2009. Where is the semantic system? A critical review and meta-analysis of 120 functional neuroimaging studies. *Cereb Cortex*. 19:2767–2796.
- Brodmann K. 1909. Vergleichende Lokalisationslehre der Großhirnrinde. Leipzig: Barth.
- Cabeza R, Ciaramelli E, Olson IR, Moscovitch M. 2008. The parietal cortex and episodic memory: an attentional account. *Nat Rev Neurosci*. 9:613–625.
- Caspers S, Eickhoff SB, Geyer S, Schepers F, Mohlberg H, Zilles K, Amunts K. 2008. The human inferior parietal lobule in stereotaxic space. *Brain Struct Funct*. 212:481–495.
- Caspers S, Eickhoff SB, Rick T, von Kapri A, Kuhlen T, Huang R, Shah NJ, Zilles K. 2011. Probabilistic fibre tract analysis of cytoarchitectonically defined human inferior parietal lobule areas reveals similarities to macaques. *Neuroimage*. 58:362–380.

- Caspers S, Geyer S, Schleicher A, Mohlberg H, Amunts K, Zilles K. 2006. The human inferior parietal cortex: cytoarchitectonic parcelation and interindividual variability. *Neuroimage*. 33:430–448.
- Caspers S, Schleicher A, Bacha-Trams M, Palomero-Gallagher N, Amunts K, Zilles K. 2013. Organization of the human inferior parietal lobule based on receptor architectonics. *Cereb Cortex*. 23:615–628.
- Caspers S, Zilles K, Laird AR, Eickhoff SB. 2010. ALE meta-analysis of action observation and imitation in the human brain. *Neuroimage*. 50:1148–1167.
- Catani M, Jones DK, Ffytche DH. 2005. Perisylvian language networks of the human brain. *Ann Neurol*. 57:8–16.
- Choi HJ, Zilles K, Mohlberg H, Schleicher A, Fink GR, Armstrong E, Amunts K. 2006. Cytoarchitectonic identification and probabilistic mapping of two distinct areas within the anterior ventral bank of the human intraparietal sulcus. *J Comp Neurol*. 495:53–69.
- Corbetta M, Shulman GL. 2002. Control of goal-directed and stimulus-driven attention in the brain. *Nat Rev Neurosci*. 3:201–215.
- Fischl B, Sereno MI, Dale AM. 1999. Cortical surface-based analysis. II: inflation, flattening, and a surface-based coordinate system. *Neuroimage*. 9:195–207.
- Friederici AD. 2009. Pathways to language: fiber tracts in the human brain. *Trends Cogn Sci*. 13:175–181.
- Gerhardt E. 1940. Die Cytoarchitektonik des Isocortex parietalis beim Menschen. *J Psychol Neurol*. 49:367–419.
- Geyer S, Luppino G, Ekamp H, Zilles K. 2005. The macaque inferior parietal lobule: cytoarchitecture and distribution pattern of serotonin 5-HT 1A binding sites. *Anat Embryol*. 210:353–362.
- Gorbach NS, Schutte C, Melzer C, Goldau M, Sujazow O, Jitsev J, Douglas T, Tittgemeyer M. 2011. Hierarchical information-based clustering for connectivity-based cortex parcellation. *Front Neuroinform*. 5:18.
- Graves WW, Desai R, Humphries C, Seidenberg MS, Binder JR. 2010. Neural systems for reading aloud: a multiparametric approach. *Cereb Cortex*. 20:1799–1815.
- Greenberg AS, Verstynen T, Chiu YC, Yantis S, Schneider W, Behrmann M. 2012. Visuotopic cortical connectivity underlying attention revealed with white-matter tractography. *J Neurosci*. 32:2773–2782.
- Gregoriou GG, Borra E, Matelli M, Luppino G. 2006. Architectonic organization of the inferior parietal convexity of the macaque monkey. *J Comp Neurol*. 496:422–451.
- Hartwigsen G, Baumgaertner A, Price CJ, Koehnke M, Ulmer S, Siebner HR. 2010. Phonological decisions require both the left and right supramarginal gyri. *Proc Natl Acad Sci USA*. 107:16494–16499.
- Humphries C, Binder JR, Medler DA, Liebenthal E. 2007. Time course of semantic processes during sentence comprehension: an fMRI study. *Neuroimage*. 36:924–932.
- Jenkinson M, Bannister P, Brady M, Smith S. 2002. Improved optimization for the robust and accurate linear registration and motion correction of brain images. *Neuroimage*. 17:825–841.
- Johansen-Berg H, Behrens TEJ, Robson MD, Dronjak I, Rushworth MFS, Brady JM, Smith SM, Higham DJ, Matthews PM. 2004. Changes in connectivity profiles define functionally distinct regions in human medial frontal cortex. *Proc Natl Acad Sci USA*. 101:13335–13340.
- Johansen-Berg H, Behrens TEJ, Sillery E, Ciccarelli O, Thompson AJ, Smith SM, Matthews PM. 2005. Functional-anatomical validation and individual variation of diffusion tractography-based segmentation of the human thalamus. *Cereb Cortex*. 15:31–39.
- Jones DK. 2010. Challenges and limitations of quantifying brain connectivity in vivo with diffusion MRI. *Imag Med*. 2:341–355.
- Jones DK, Knösche TR, Turner R. 2013. White matter integrity, fiber count, and other fallacies: The do's and don'ts of diffusion MRI. *Neuroimage*. 73:239–254.
- Kelly C, Uddin LQ, Shehzad Z, Margulies DS, Castellanos FX, Milham MP, Petrides M. 2010. Broca's region: linking human brain functional connectivity data and non-human primate tracing anatomy studies. *Eur J Neurosci*. 32:383–398.
- Klein JC, Behrens TEJ, Robson MD, Mackay CE, Higham DJ, Johansen-Berg H. 2007. Connectivity-based parcellation of human cortex using diffusion MRI: establishing reproducibility, validity and observer independence in BA 44/45 and SMA/pre-SMA. *Neuroimage*. 34:204–211.
- Mars RB, Jbabdi S, Sallet J, O'Reilly JX, Croxson PL, Olivier E, Noonan MP, Bergmann C, Mitchell AS, Baxter MG et al. 2011. Diffusion-weighted imaging tractography-based parcellation of the human parietal cortex and comparison with human and macaque resting-state functional connectivity. *J Neurosci*. 31:4087–4100.
- Obleser J, Boecker H, Drzezga A, Haslinger B, Hennenlotter A, Roettger M, Eulitz C, Rauschecker JP. 2006. Vowel sound extraction in anterior superior temporal cortex. *Hum Brain Mapp*. 27:562–571.
- Ono M, Kubik S, Abernathey CD. 1990. *Atlas of the cerebral sulci*. Stuttgart: Thieme.
- Pandya DN, Seltzer B. 1982. Intrinsic connections and architectonics of posterior parietal cortex in the rhesus monkey. *J Comp Neurol*. 204:196–210.
- Price CJ. 2010. The anatomy of language: a review of 100 fMRI studies published in 2009. *Ann N Y Acad Sci*. 1191:62–88.
- Rizzolatti G, Craighero L. 2004. The mirror-neuron system. *Annu Rev Neurosci*. 27:169–192.
- Rozzi S, Calzavara R, Belmalih A, Borra E, Gregoriou GG, Matelli M, Luppino G. 2006. Cortical connections of the inferior parietal cortical convexity of the macaque monkey. *Cereb Cortex*. 16:1389–1417.
- Rozzi S, Ferrari PF, Bonini L, Rizzolatti G, Fogassi L. 2008. Functional organization of inferior parietal lobule convexity in the macaque monkey: electrophysiological characterization of motor, sensory and mirror responses and their correlation with cytoarchitectonic areas. *Eur J Neurosci*. 28:1569–1588.
- Rushworth MFS, Behrens TEJ, Johansen-Berg H. 2006. Connection patterns distinguish 3 regions of human parietal cortex. *Cereb Cortex*. 16:1418–1430.
- Sakai KL, Hashimoto R, Homae F. 2001. Sentence processing in the cerebral cortex. *Neurosci Res*. 39:1–10.
- Sarkissova SA, Filimonoff IN, Kononova EP, Preobraschenskaja IS, Kukuev LA. 1955. *Atlas of the cytoarchitectonics of the human cerebral cortex*. Moscow: Medgiz.
- Schleicher A, Amunts K, Geyer S, Morosan P, Zilles K. 1999. Observer-independent method for microstructural parcellation of cerebral cortex: a quantitative approach to cytoarchitectonics. *Neuroimage*. 9:165–177.
- Schmahmann JD, Pandya DN. 2006. *Fiber pathways of the brain*. Oxford: Oxford University Press.
- Schmahmann JD, Pandya DN, Wang R, Dai G, D'Arceuil HE, de Crespiigny AJ, Wedeen VJ. 2007. Association fibre pathways of the brain: Parallel observations from diffusion spectrum imaging and autoradiography. *Brain*. 130:630–653.
- Schubotz RI, Anwander A, Knösche TR, von Cramon DY, Tittgemeyer M. 2010. Anatomical and functional parcellation of the human lateral premotor cortex. *Neuroimage*. 50:396–408.
- Seltzer B, Pandya DN. 1984. Further observations on parieto-temporal connections in the rhesus monkey. *Exp Brain Res*. 55:301–312.
- Thiebaut de Schotten M, Dell'Acqua F, Forkel SJ, Simmons A, Vergani F, Murphy DG, Catani M. 2011. A lateralized brain network for visuospatial attention. *Nat Neurosci*. 14:1245–1246.
- Tomassini V, Jbabdi S, Klein JC, Behrens TEJ, Pozzilli C, Matthews PM, Rushworth MFS, Johansen-Berg H. 2007. Diffusion-weighted imaging tractography-based parcellation of the human lateral premotor cortex identifies dorsal and ventral subregions with anatomical and functional specializations. *J Neurosci*. 27:10259–10269.
- Umarova RM, Saur D, Kaller CP, Vry MS, Glauche V, Mader I, Hennig J, Weiller C. 2011. Acute visual neglect and extinction: distinct functional state of the visuospatial attention system. *Brain*. 134:3310–3325.
- Vigneau M, Beaucousin V, Herve PY, Duffau H, Crivello F, Houde O, Mazoyer B, Tzourio-Mazoyer N. 2006. Meta-analyzing left hemisphere language areas: phonology, semantics, and sentence processing. *Neuroimage*. 30:1414–1432.
- Vilberg KL, Rugg MD. 2008. Memory retrieval and the parietal cortex: a review of evidence from a dual-process perspective. *Neuropsychologia*. 46:1787–1799.

- Vogt C, Vogt O. 1919. Allgemeine Ergebnisse unserer Hirnforschung. *J Psychol Neurol.* 25:279–461.
- Vogt O. 1911. Die Myeloarchitektonik des Isocortex parietalis. *J Psychol Neurol.* 18:379–390.
- von Bonin G, Bailey P. 1947. *The neocortex of Macaca Mulatta*. Urbana (IL): University of Illinois Press.
- von Economo K, Koskinas G. 1925. *Die Cytoarchitektonik der Hirnrinde des erwachsenen Menschen*. Wien: Springer.